Ideal Weyl Semimetals in the Chalcopyrites CuTlSe_{2}, AgTlTe_{2}, AuTlTe_{2}, and ZnPbAs_{2}

Jiawei Ruan, Shao-Kai Jian, Dongqin Zhang, Hong Yao, Haijun Zhang, Shou-Cheng Zhang, and Dingyu Xing

Ideal Weyl semimetals in the chalcopyrites CuTlSe$_2$, AgTlTe$_2$, AuTlTe$_2$ and ZnPbAs$_2$

Jiawei Ruan[1,†], Shao-Kai Jian[2,†], Dongqin Zhang[1], Hong Yao[2,3], Haijun Zhang[1], Shou-Cheng Zhang[4], Dingyu Xing[1]

[1] *National Laboratory of Solid State Microstructures, School of Physics,*
and Collaborative Innovation Center of Advanced Microstructures, Nanjing University, Nanjing 210093, China
[2] *Institute for Advanced Study, Tsinghua University, Beijing 100084, China*
[3] *Collaborative Innovation Center of Quantum Matter, Beijing 100084, China*
[4] *Department of Physics, McCullough Building, Stanford University, Stanford, CA 94305-4045, USA*
(Dated: May 13, 2016)

Weyl semimetals are new states of matter which feature novel Fermi arcs and exotic transport phenomena. Based on first-principles calculations, we report that the chalcopyrites CuTlSe$_2$, AgTlTe$_2$, AuTlTe$_2$ and ZnPbAs$_2$ are ideal Weyl semimetals, having largely separated Weyl points ($\sim 0.05 \text{Å}^{-1}$) and uncovered Fermi arcs that are amenable to experimental detections. We also construct a minimal effective model to capture the low-energy physics of this class of Weyl semimetals. Our discovery is a major step toward a perfect playground of intriguing Weyl semimetals and potential applications for low-power and high-speed electronics.

PACS numbers: 73.20.At,71.55.Ak,73.43.-f

Weyl fermions, originally introduced as massless chiral fermions, are described by the Weyl equation[1]. Even though a number of elementary particles were considered as candidates of Weyl fermions, conclusive evidences of Weyl fermions as elementary particles are still lacking. Weyl fermions were also proposed as emergent low-energy quasiparticles in condensed matter systems breaking either time-reversal or spatial-inversion symmetry [2–16]. One hallmark of Weyl semimetals is the existence of Fermi arcs in surface states[3]. So far the only experimentally known Weyl semimetals are the TaAs-class compounds, in which two sets of inequivalent Weyl points away from the Fermi level and complex Fermi surfaces were found by ARPES experiments[17–19]. Experimental evidences of negative magnetoresistance[2, 20] induced by the chiral anomaly were also reported[21–26]. However, definite signatures of the chiral anomaly in the quantum limit, such as the linear-B negative magnetoresistance[2, 20, 27] and the emergent supersymmetry[28], and others[29–32] haven't been experimentally observed in known Weyl semimetals, which is partly due to the facts that the Weyl points are not all at the Fermi level and that there are coexisting trivial Fermi pockets. Therefore, it is urgent to discover ideal Weyl semimetals with *only* symmetry-related Weyl points at the Fermi level.

In this work, we focus on a large family of ternary chalcopyrites ABC$_2$ at stoichiometry, which were of great interest because of potential applications including the thermoelectric effect, non-linear optics and solar cells[33, 34]. Recently, some ternary chalcopyrites were predicted to be topological insulators[35]. Here, our first-principles calculations find that the chalcopyrite compounds CuTlSe$_2$, AgTlTe$_2$, AuTlTe$_2$ and ZnPbAs$_2$ are a class of ideal Weyl semimetals having eight symmetry-related Weyl points exactly at the Fermi level, but without any fine tuning. CuTlTe$_2$ and ZnPbSb$_2$ are also Weyl semimetals having eight symmetry-related
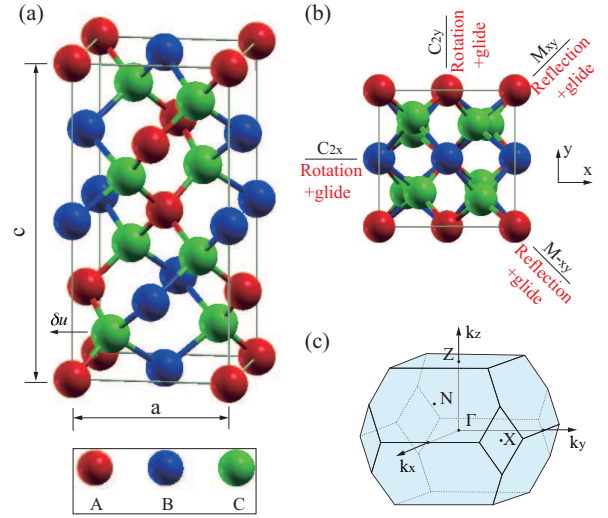

FIG. 1. Crystal structure and Brillouin zone (BZ). (a) The crystal structure of chalcopyrite compounds ABC$_2$, including CuTlSe$_2$, CuTlTe$_2$, AgTlTe$_2$, AuTlTe$_2$, ZnPbAs$_2$ and ZnPbSb$_2$. The deviation of C atom (green) away from the center of tetrahedron formed by A and B atoms is denoted by δu. (b) The top view of the chalcopyrite structure. The two-fold rotation symmetries (C_{2x} and C_{2y}) and the two mirror symmetries (M_{xy} and M_{-xy}) are marked. (c) The BZ of chalcopyrite compounds.

Weyl points in energy gaps but have a few coexisting trivial bands around the X point; consequently they are not ideal Weyl semimetals at stoichiometry but can be tuned to be ideal Weyl semimetals by gating or doping. The ideal Weyl semimetals predicted in the chalcopyrites are analogous to those in compressively strained HgTe and half-Heusler compounds[16], but have one important advantage: external strain is no longer needed to realize ideal Weyl semimetal phases in these chalcopyrites. The surface Fermi arcs of these Weyl semimetals on both the (001) and (010) surfaces are uncovered and
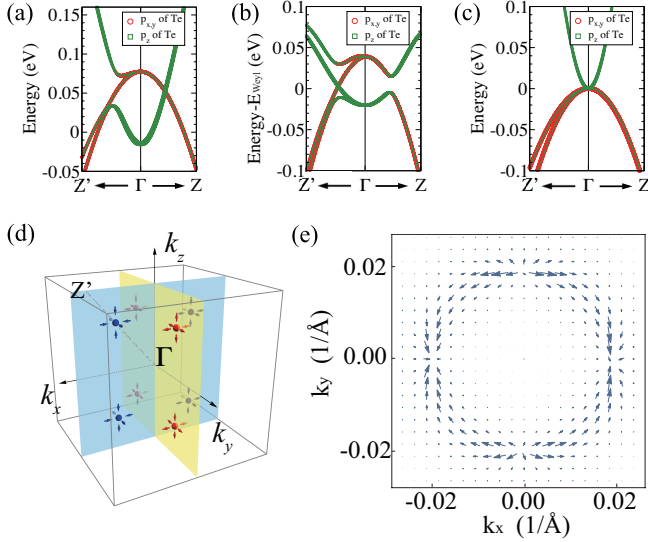
FIG. 2. Band structure and Weyl points. (a) The bands of CuTlTe$_2$ without turning on the spin-orbit coupling (SOC) effect. The p_z bands are below $p_{x,y}$ bands at the Γ point. (b) The bands of CuTlTe$_2$ with turning on the SOC effect. An energy gap opens along the line of Γ-Z, and one Weyl point is seen between Γ and Z'. E$_{Weyl}$ denotes the energy level of Weyl points. (c) The bands of Hg$_2$Te$_2$ without turning on the SOC effect at the Γ point are three-fold degenerate protected by the cubic symmetry. (d) The schematic eight symmetry-related Weyl points in the BZ. (e) Berry curvature in a k_z plane including four Weyl points. The Weyl points at $(\pm k_x^*, 0, \pm k_z^*)$ have the '-1' chirality and at $(0, \pm k_y^*, \pm k_z^*)$ have '$+1$' chirality.

FIG. 3. Surface states and Fermi arcs. (a) The local density of states (LDOS) for CuTlTe$_2$ projected onto the (001) surface. The warmer colors represent higher LDOS. The red/blue regions indicate bulk bands/energy gaps, and the single red lines indicate the surface states. The bulk band crossing ($\bar{k}_x^*$, 0), projected from the two Weyl points (k_x^*, 0, $\pm k_z^*$), can be seen in the $\bar{\Gamma}$-$\bar{X}$ line. The velocities of surface states along $\bar{\Gamma}$-$\bar{M}_1$ and $\bar{\Gamma}$-$\bar{M}_2$ have opposite sign. (b) A closed Fermi surface consists of four Fermi arcs in the (001) surface. The high-symmetry lines in (a) are marked. (c) The open Fermi arcs on the (010) surface. (d) The zoomed-in Fermi arcs of (c).

are amenable to ARPES detections. Such ideal Weyl semimetals provide a promising arena to observe the weak-field linear-B negative magneto-resistance[2, 36], a signature of the chiral anomaly in the quantum limit, which is still in debate so far.

Electronic structures

The chalcopyrite compounds share a body-centered-tetragonal (bct) crystal structure with the space group D_{2d}^{12} ($I\bar{4}2d$) which could be obtained by doubling the zinc-blende structure along the z direction, such that its lattice constant c is about twice of a, as shown in Fig. 1a. It has two twofold rotation symmetries C_{2x} and C_{2y} and two mirror symmetries M_{xy} and M_{-xy} combining with a proper glide (Fig. 1b). Generally, in the structure of chalcopyrites ABC$_2$, two A and two B atoms form a tetrahedron surrounding one C atom. The tetrahedron is slightly tetragonally distorted, characterized by the ratio of the lattice constants $\eta = c/2a$, and the C atoms is off the center of the tetrahedron, characterized by $\delta u = (R_{AC}^2 - R_{BC}^2)/a^2$ where R_{AC} and R_{BC} denote the distance between C and its nearest A and B atoms respectively. Heuristically, the zinc-blende HgTe can be regarded as a special "chalcopyrite" ABC$_2$ with A=Hg,
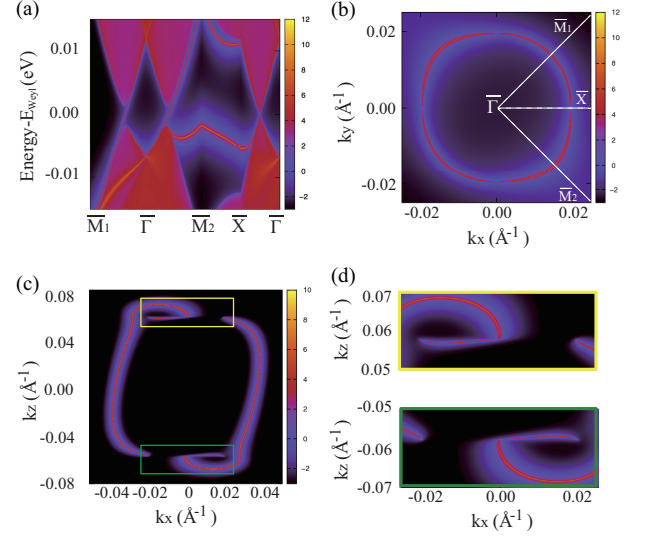
B=Hg, C=Te, $\eta = 1$, and $\delta u = 0$. Interestingly, the chalcopyrite compounds ABC$_2$, where the cubic symmetry is broken due to the tetragonal distortion ($\eta \neq 1$) and the internal displacement ($\delta u \neq 0$), can be effectively considered as a strained HgTe.

The I-III-VI$_2$ and II-IV-V$_2$ chalcopyrite compounds have sixteen valence electrons per unit cell, naively indicating an insulating ground state, which is true for CuInS$_2$ and ZnGeAs$_2$. However, an sp-type band inversion[37], like in HgTe, exists in many I-III-VI$_2$ and II-IV-V$_2$ chalcopyrite compounds, which can give rise to topologically nontrivial state[35]. Notably, as the chalcopyrite structure is effectively similar to a strained zinc-blende structure, those chalcopyrite compounds with the nontrivial band inversion are expected to realize topological insulators or ideal Weyl semimetals, depending on the type of the effective strain[16]. Indeed, our first-principles calculations show that CuTlSe$_2$, AgTlTe$_2$, AuTlTe$_2$ and ZnPbAs$_2$ are ideal Weyl semimetals with eight symmetry-related Weyl points at the Fermi level, and CuTlTe$_2$ and ZnPbSb$_2$ are also Weyl semimetals with eight symmetry-related Weyl points but coexisting with trivial Fermi pockets. Four pairs of Weyl points are pinned either in the $k_x = 0$ or $k_y = 0$ plane because of crystal symmetries, schematically shown in Fig. 2d.

Without loss of generality, we take CuTlTe$_2$ as an ex-

ample to show the unique feature of symmetry-protected Weyl points in topologically nontrivial chalcopyrite compounds I-III-VI$_2$ and II-IV-V$_2$. The band inversion between the s bands of Cu and Tl and the p bands of Te around Γ, which makes the p bands of Te dominate the Fermi level, is shown in Fig. 2a and b. The bands of CuTlTe$_2$ are very similar to those of HgTe (equivalently Hg$_2$Te$_2$), except some features due to the tetragonal distortion in the chalcopyrite structure ($\eta \neq 1$ and $\delta u \neq 0$). We can see that the top of valence bands of Hg$_2$Te$_2$, without turning on the SOC effect, are three-fold degenerate, indicating the degeneracy of p_x, p_y and p_z orbitals at the Γ point, shown in Fig. 2c. Contrastively, in CuTlTe$_2$, the top of valence bands at Γ split into two-fold degenerate bands ($p_{x,y}$) and one single band (p_z), shown in Fig. 2a, which indicates an effective tensile uniaxial strain along the c direction. Therefore, CuTlTe$_2$ is expected to be an ideal Weyl semimetal, like the strained HgTe[16]. The Weyl point is really seen in the bands of CuTlTe$_2$ (Fig. 2b). There are totally eight Weyl points which are all related to each other by symmetries, schematically shown in Fig. 2d. They are confined in $k_x = 0$ or $k_y = 0$ planes by the $C_{2T} = C_2 \cdot T$ symmetry, where C_2 denotes a two-fold rotation C_{2x} or C_{2y}, and T denotes the time-reversal symmetry. The four Weyl points in the $k_x = 0$ ($k_y = 0$) plane have the same chirality, for example, '+1' ('−1') in Fig. 2d and e.

Surface states and Fermi arcs
The existence of topologically protected Fermi arcs is one hallmark of Weyl semimetals. We calculate the surface states and Fermi arcs of CuTlTe$_2$ through the maximally localized Wannier functions on the basis of first-principles calculations. The local density of states (LDOS) on the (001) surface is shown in Fig. 3a. One touching point ($\bar{k}_x^*$, 0) in the $\bar{X}$-$\bar{\Gamma}$, projected from the two Weyl points (k_x^*, 0, $\pm k_z^*$), has a monopole charge '−2'. Similarly, the touching point ($-\bar{k}_x^*$, 0) also has a monopole charge '−2', while both $(0, \pm \bar{k}_y^*)$ have a monopole charge '+2'. Therefore, one cannot see open Fermi arcs on the (001) surface Fermi surface because of the monopole charges of ± 2. We calculate the Fermi arcs on the (001) surface, shown in Fig. 3b, where a closed Fermi surface consisting of four individual Fermi arcs is presented. Most interestingly, the surface states have the velocities of opposite sign along $\bar{\Gamma}$-$\bar{M}_1$ and $\bar{\Gamma}$-$\bar{M}_2$, shown in Fig. 3a, indicating that the closed Fermi surface consisting of four Fermi arcs is topological different from the surface state of topological insulators such as Bi$_2$Se$_3$[38], where two Fermi velocities along $\bar{\Gamma}$-$\bar{M}_1$ and $\bar{\Gamma}$-$\bar{M}_2$ have the same sign.

On the (010) surface, there are six gapless points, including four points $(\pm \bar{k}_x^*, \pm \bar{k}_z^*)$ with the monopole charge '−1', and two points $(0, \pm \bar{k}_z^*)$ with the monopole charge '+2'. The open Fermi arcs emerge, as shown in Fig. 3c, and the zoomed-in parts of Fermi arcs are shown in Fig. 3d. The Fermi arcs are consistent with those in
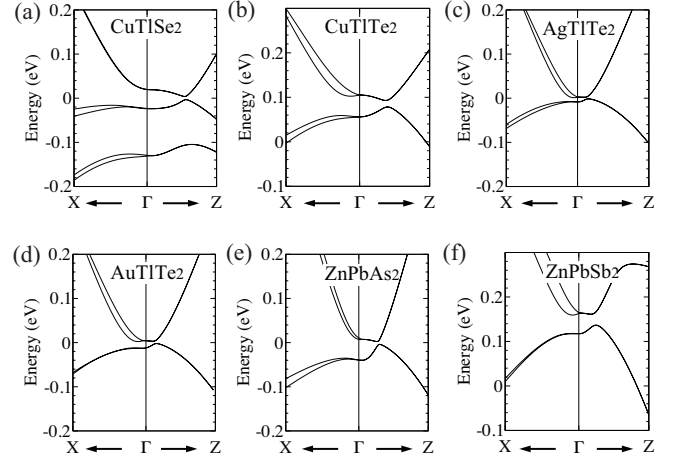

FIG. 4. Band structures of Weyl semimetal candidates. (a-f) The band structures with turning on the SOC effect by the mBJ calculations for CuTlSe$_2$ (a), CuTlTe$_2$ (b), AgTlTe$_2$ (c), AuTlTe$_2$ (d), ZnPbAs$_2$ (e) and ZnPbSb$_2$ (f).

strained HgTe [16]. However, it is worth noticing that the Weyl points here are well separated, for example, about 5% of the reciprocal lattice constant between the two Weyl points $(\pm k_x^*, 0, k_z^*)$, which is much amenable for experimental detections.

Weyl semimetal candidates
In Fig. 4, based on the modified Becke-Johnson (mBJ) calculations, the bulk band structures of six chalcopyrite compounds CuTlSe$_2$, CuTlTe$_2$, AgTlTe$_2$, AuTlTe$_2$, ZnPbAs$_2$, and ZnPbSb$_2$, are shown, exhibiting similar band structures. Based on our calculations, they are all Weyl semimetals with eight symmetry-protected Weyl points, especially including four ideal Weyl semimetals CuTlSe$_2$, AgTlTe$_2$, AuTlTe$_2$, and ZnPbAs$_2$. For CuTlTe$_2$ and ZnPbSb$_2$, the bottom of the conduction bands stays around the X point at the boundary of the BZ (seen in Fig. S2c in the supplementary information(SI)) which is far from the Γ point. Therefore, although there are trivial bulk bands coexisting with the Weyl points, the Weyl points are still well separated from the trivial bands in CuTlTe$_2$ and ZnPbSb$_2$. For all these six Weyl semimetals, the positions of Weyl points $(\pm k_x^*, 0, \pm k_z^*)$ and $(0, \pm k_y^*, \pm k_z^*)$ are calculated by both standard GGA and mBJ calculations, listed in Table S1 in SI. We can see that the larger difference in atomic radius between A and B atoms in chalcopyrites ABC$_2$ produces the larger k_z^* for Weyl points, and the larger SOC effect of C atom results in larger $k_{x,y}^*$. Consequently, Weyl points of CuTlTe$_2$ and ZnPbSb$_2$ are the most separated among these materials.

Low-energy effective model
The topological nature in these ideal Weyl semimetals is determined mainly by the low-energy physics near the

Weyl points, which can be captured by a low-energy effective Hamiltonian. Up to the quadratic order of momenta $\mathbf{k}$, the low-energy effective model can be explicitly written down under the restriction to the time-reversal symmetry and the lattice symmetry (D_{2d}), as shown in SI. Interestingly, we can reach an analytically-trackable low-energy effective model which can capture the topological features of these ideal Weyl semimetals:

$$H(\mathbf{k}) = \epsilon_0(\mathbf{k})I_{4\times4} + c_1(k_yk_z\Gamma^1 + k_zk_x\Gamma^2) + c_2k_xk_y\Gamma^3 \quad (1)$$
$$+c_4(k_x^2 - k_y^2)\Gamma^4 + \left[c_3(k_z^2 - m^2) + c_5(k_x^2 + k_y^2)\right]\Gamma^5 + vk_z\Gamma^{35},$$

where $\epsilon_0(\mathbf{k}) = a_0 + a_1(k_x^2 + k_y^2) + a_2k_z^2$, Γ^i are 4×4 matrices given in the SI, and c_i, a_i, m, v are constants. The effective model can be understood by lowering the symmetry of Luttinger Hamiltonian. The $m^2\Gamma^5$ and $k_z\Gamma^{35}$ terms break reflection and inversion symmetries, respectively, rendering a quadratic band-touching to split into eight Weyl points in the high-symmetry plane as stated before. The eigen-energy reads $E(\mathbf{k}) = \epsilon_0(\mathbf{k}) \pm \left[d_1^2(\mathbf{k}) + d_2^2(\mathbf{k}) + d_3^2(\mathbf{k})\right]^{\frac{1}{2}}$, where $d_i(\mathbf{k})$ are given in the SI. There are eight Weyl points in this effective Hamiltonian whose locations are given in the SI for certain range of parameters. The projected Hamiltonian near one of the Weyl points is described by the Weyl equations, i.e.,

$$H_{\text{Weyl}}(\mathbf{k}) = -c_1mk_x\sigma^x + \frac{c_2v}{c_1}k_y\sigma^y + 2c_3mk_z\sigma^z, \quad (2)$$

where the identity matrix part is neglected because it does not affect the topological properties. Since the low-energy physics is captured by the locations and the Fermi velocities of the Weyl points which can be determined uniquely by the the effective model, it correctly captures the low-energy physics in this class of Weyl semimetals.

[1] H. Weyl, Z. Phys. **56**, 330 (1929).

[2] H. B. Nielsen and M. Ninomiya, Physics Letters B **130**, 389 (1983).

[3] X. Wan, A. M. Turner, A. Vishwanath, and S. Y. Savrasov, Phys. Rev. B **83**, 205101 (2011).

[4] G. Xu, H. Weng, Z. Wang, X. Dai, and Z. Fang, Phys. Rev. Lett. **107**, 186806 (2011).

[5] A. A. Burkov and L. Balents, Phys. Rev. Lett. **107**, 127205 (2011).

[6] A. A. Zyuzin and A. A. Burkov, Phys. Rev. B **86**, 115133 (2012).

[7] K.-Y. Yang, Y.-M. Lu, and Y. Ran, Phys. Rev. B **84**, 075129 (2011).

[8] G. B. Halász and L. Balents, Phys. Rev. B **85**, 035103 (2012).

[9] P. Hosur and X. Qi, Comptes Rendus Physique **14**, 857 (2013).

[10] H. Zhang, J. Wang, G. Xu, Y. Xu, and S.-C. Zhang, Phys. Rev. Lett. **112**, 096804 (2014).

[11] J. Liu and D. Vanderbilt, Phys. Rev. B **90**, 155316 (2014).

[12] H. Weng, C. Fang, Z. Fang, B. A. Bernevig, and X. Dai, Phys. Rev. X **5**, 011029 (2015).

[13] S.-M. Huang, S.-Y. Xu, I. Belopolski, C.-C. Lee, G. Chang, B. Wang, N. Alidoust, G. Bian, M. Neupane, C. Zhang, S. Jia, A. Bansil, H. Lin, and M. Z. Hasan, Nature Communications **6**, 7373 (2015).

[14] A. A. Soluyanov, D. Gresch, Z. Wang, Q. Wu, M. Troyer, X. Dai, and B. A. Bernevig, Nature **527**, 495 (2015).

[15] M. Hirayama, R. Okugawa, S. Ishibashi, S. Murakami, and T. Miyake, Phys. Rev. Lett. **114**, 206401 (2015).

[16] J. Ruan, S.-K. Jian, H. Yao, H. Zhang, S.-C. Zhang, and D. Xing, arXiv:1511.08284 (2015).

[17] L. X. Yang, Z. K. Liu, Y. Sun, H. Peng, H. F. Yang, T. Zhang, B. Zhou, Y. Zhang, Y. F. Guo, M. Rahn, D. Prabhakaran, Z. Hussain, S. K. Mo, C. Felser, B. Yan, and Y. L. Chen, Nature Physics **11**, 728 (2015).

[18] B. Q. Lv, H. M. Weng, B. B. Fu, X. P. Wang, H. Miao, J. Ma, P. Richard, X. C. Huang, L. X. Zhao, G. F. Chen, Z. Fang, X. Dai, T. Qian, and H. Ding, Phys. Rev. X **5**, 031013 (2015).

[19] S.-Y. Xu, I. Belopolski, N. Alidoust, M. Neupane, G. Bian, C. Zhang, R. Sankar, G. Chang, Z. Yuan, C.-C. Lee, S.-M. Huang, H. Zheng, J. Ma, D. S. Sanchez, B. Wang, A. Bansil, F. Chou, P. P. Shibayev, H. Lin, S. Jia, and M. Z. Hasan, Science **349**, 613 (2015).

[20] D. T. Son and B. Z. Spivak, Phys. Rev. B **88**, 104412 (2013).

[21] X. Huang, L. Zhao, Y. Long, P. Wang, D. Chen, Z. Yang, H. Liang, M. Xue, H. Weng, Z. Fang, X. Dai, and G. Chen, Phys. Rev. X **5**, 031023 (2015).

[22] X. Yang, Y. Liu, Z. Wang, Y. Zheng, and Z. an Xu, arXiv:1506.03190 (2015).

[23] C. Shekhar, F. Arnold, S.-C. Wu, Y. Sun, M. Schmidt, N. Kumar, A. G. Grushin, J. H. Bardarson, R. Donizeth dos Reis, M. Naumann, M. Baenitz, H. Borrmann, M. Nicklas, E. Hassinger, C. Felser, and B. Yan, arXiv:1506.06577 (2015).

[24] J. Xiong, S. K. Kushwaha, T. Liang, J. W. Krizan, M. Hirschberger, W. Wang, R. J. Cava, and N. P. Ong, Science **350**, 413 (2015).

[25] H. Li, H. He, H.-Z. Lu, H. Zhang, H. Liu, R. Ma, Z. Fan, S.-Q. Shen, and J. Wang, ArXiv e-prints (2015), arXiv:1507.06470.

[26] C.-Z. Li, L.-X. Wang, H. Liu, J. Wang, Z.-M. Liao, and D.-P. Yu, ArXiv e-prints (2015), arXiv:1504.07398.

[27] S.-B. Zhang, H.-Z. Lu, and S.-Q. Shen, ArXiv e-prints (2015), arXiv:1509.02001.

[28] S.-K. Jian, Y.-F. Jiang, and H. Yao, Phys. Rev. Lett. **114**, 237001 (2015).

[29] H. Wei, S.-P. Chao, and V. Aji, Phys. Rev. Lett. **109**, 196403 (2012).

[30] C.-X. Liu, P. Ye, and X.-L. Qi, Phys. Rev. B **87**, 235306 (2013).

[31] P. E. C. Ashby and J. P. Carbotte, Phys. Rev. B **87**, 245131 (2013).

[32] X.-Q. Sun, S.-C. Zhang, and Z. Wang, Phys. Rev. Lett. **115**, 076802 (2015).

[33] J. L. Shay and J. H. Wernick, *Ternary Chalcopyrite Semiconductors: Growth, Electronic Properties and Applications* (Pergamon Press, Oxford, 1975).

[34] S. Wei and A. Zunger, Journal of Applied Physics **78**, 3846 (1995).

[35] W. Feng, D. Xiao, J. Ding, and Y. Yao, Phys. Rev. Lett. **106**, 016402 (2011).

[36] C. Zhang, S.-Y. Xu, I. Belopolski, Z. Yuan, Z. Lin, B. Tong, N. Alidoust, C.-C. Lee, S.-M. Huang, H. Lin, M. Neupane, D. S. Sanchez, H. Zheng, G. Bian, J. Wang, C. Zhang, T. Neupert, M. Zahid Hasan, and S. Jia, ArXiv e-prints (2015), arXiv:1503.02630.

[37] H. Zhang and S.-C. Zhang, Phys. Status solidi RRL **7**, 72 (2013).

[38] H. Zhang, C.-X. Liu, X.-L. Qi, X. Dai, Z. Fang, and S.-C. Zhang, Nature Physics **5**, 438 (2009).

[supp] See Supplemental Material [url], which includes Refs. [40-48].

[40] Z. Fang and K. Terakura, J. Phys.: Condens. Matter **14**, 3001 (2002).

[41] F. Tran and P. Blaha, Phys. Rev. Lett. **102**, 226401 (2009).

[42] G. Kresse and J. Furthmüller, Phys. Rev. B **54**, 11169 (1996).

[43] N. Marzari and D. Vanderbilt, Phys. Rev. B **56**, 12847 (1997).

[44] I. Souza, N. Marzari, and D. Vanderbilt, Phys. Rev. B **65**, 035109 (2001).

[45] H.-J. Zhang, C.-X. Liu, X.-L. Qi, X.-Y. Deng, X. Dai, S.-C. Zhang, and Z. Fang, Phys. Rev. B **80**, 085307 (2009).

[46] M. P. L. Sancho, J. M. L. Sancho, and J. Rubio, Journal of Physics F: Metal Physics **14**, 1205 (1984).

[47] M. P. L. Sancho, J. M. L. Sancho, J. M. L. Sancho, and J. Rubio, Journal of Physics F: Metal Physics **15**, 851 (1985).

[48] S. Murakami, N. Nagaosa, and S.C. Zhang, Phys. Rev. B **69**, 235206 (2004).